Crystal Structure of Adenosine 5′-Phosphosulfate Kinase from *Penicillium chrysogenum*[†,‡]

Ian J. MacRae,[§] Irwin H. Segel,[§] and Andrew J. Fisher*[,§,||]

Department of Chemistry and Section of Molecular and Cellular Biology, University of California, One Shields Avenue, Davis, California 95616

Received October 18, 1999

ABSTRACT: Adenosine 5′-phosphosulfate (APS) kinase catalyzes the second reaction in the two-step conversion of inorganic sulfate to 3′-phosphoadenosine 5′-phosphosulfate (PAPS). This report presents the 2.0 Å resolution crystal structure of ligand-free APS kinase from the filamentous fungus, *Penicillium chrysogenum*. The enzyme crystallized as a homodimer with each subunit folded into a classic kinase motif consisting of a twisted, parallel β-sheet sandwiched between two α-helical bundles. The Walker A motif, ^{32}GLSASGKS^{39}, formed the predicted P-loop structure. Superposition of the APS kinase active site region onto several other P-loop-containing proteins revealed that the conserved aspartate residue that usually interacts with the Mg^{2+} coordination sphere of MgATP is absent in APS kinase. However, upon MgATP binding, a different aspartate, Asp 61, could shift and bind to the Mg^{2+}. The sequence ^{156}KAREGVIKEFT^{166}, which has been suggested to be a (P)APS motif, is located in a highly protease-susceptible loop that is disordered in both subunits of the free enzyme. MgATP or MgADP protects against proteolysis; APS alone has no effect but augments the protection provided by MgADP. The results suggest that the loop lacks a fixed structure until MgATP or MgADP is bound. The subsequent conformational change together with the potential change promoted by the interaction of MgATP with Asp 61 may define the APS binding site. This model is consistent with the obligatory ordered substrate binding sequence (MgATP or MgADP before APS) as established from steady state kinetics and equilibrium binding studies.

The activation of inorganic sulfate to 3′-phosphoadenosine 5′-phosphosulfate (PAPS)[1] proceeds in two steps that are catalyzed, in order, by ATP sulfurylase (MgATP:sulfate adenylyltransferase, EC 2.7.7.4) and APS kinase (MgATP: APS 3′-phosphotransferase, EC 2.7.1.25):

$$\text{MgATP} + \text{SO}_4^{2-} \rightleftharpoons \text{MgPP}_i + \text{APS (ATP sulfurylase)}$$

$$\text{MgATP} + \text{APS} \rightleftharpoons \text{PAPS} + \text{MgADP (APS kinase)}$$

In many bacteria, yeast, and fungi, PAPS is the substrate for a reductive assimilation pathway leading to the biosynthesis of cysteine and, eventually, to all organic sulfur-containing biomolecules. Plants use APS as the activated form of sulfate for reduction. Animals do not synthesize sulfur amino acids from inorganic sulfate, but still produce PAPS that is used as the sulfuryl donor in the formation of sulfate esters.

This study focuses on APS kinase from the filamentous fungus, *Penicillium chrysogenum*, an enzyme possessing several features that make it an ideal subject for structure determination. For example, the native enzyme is a dimer composed of identical 23.67 kDa subunits (211 amino acid residues). At temperatures above ca. 42 °C, the enzyme dissociates into stable but inactive monomers. Upon cooling to ≤30 °C, the monomers reassociate forming active dimers (*1*). These observations prompt two questions. (a) What contacts stabilize the APS kinase dimer? (b) Does the active site reside at the dimer interface?

The kinetic mechanism of fungal APS kinase is compulsory ordered; MgATP adds before APS, and PAPS leaves before MgADP (*2*). The facile formation of a dead-end E·MgADP·APS complex leads to substrate inhibition by APS. The observation that APS will not bind to the free enzyme in the absence of MgATP or MgADP (*3*, *4*) suggests that this obligate order is structurally based, not just a kinetic (preferred pathway) phenomenon. Another objective then was to determine whether there was any feature of the APS kinase structure that would explain the induced binding of APS.

Finally, Satishchandran et al. (*5*−*7*) reported that the reaction catalyzed by *Escherichia coli* APS kinase proceeded via a phosphoenzyme intermediate. The phosphoryl acceptor

[†] This work is supported in part by NSF Grant MCB-9904003 to I.H.S. and A.J.F. and the W. M. Keck Foundation Center for Structural Biology at the University of California, Davis.

[‡] Protein coordinates have been deposited in the Protein Data Bank (file name 1D6J).

* To whom correspondence should be addressed: Department of Chemistry and Section of Molecular and Cellular Biology, University of California, One Shields Avenue, Davis, CA 95616. E-mail: fisher@chem.ucdavis.edu. Phone: (530) 754-6180. Fax: (530) 752-8995.

[§] Section of Molecular and Cellular Biology.

[||] Department of Chemistry.

[1] Abbreviations: APS, adenosine 5′-phosphosulfate (adenylyl sulfate); PAPS, 3′-phosphoadenosine 5′-phosphosulfate (adenylylsufate 3′-phosphate); HEPPS, *N*-(2-hydroxyethyl)piperazine-*N*′-3-propanesulfonic acid; MES, 2-(4-morpholino)ethanesulfonic acid; SDS, sodium dodecyl sulfate; DTT, dithiothreitol; ATP-γ-S, adenosine 5′-*O*-(3-thiotriphosphate); GMP, guanosine 5′-monophosphate; MgATP and MgADP, magnesium complexes of adenosine 5′-triphosphate and adenosine 5′-diphosphate, respectively. Such solutions contain the indicated concentration of nucleotide and a fixed 5 mM excess of $MgCl_2$ at pH 8.0.

10.1021/bi9924157 CCC: $19.00
Published on Web 02/15/2000

was identified as Ser 109 (analogous to Ser 107 in the fungal enzyme). Recent mutagenesis experiments (*8*) eliminated Ser 107 as an obligatory phosphoryl acceptor in the *P. chrysogenum* enzyme, but chemical modification and inactivation protection studies on the Ser 107 Cys mutant suggested that residue 107 is located in the vicinity of the active site. So the third objective of this study was to obtain direct evidence bearing on the location of Ser 107.

Although the sequences of APS kinases from about 20 different sources have been reported, no structure has been presented to date. In this report, we present the structure of the free enzyme determined to 2.0 Å resolution.

EXPERIMENTAL PROCEDURES

Protein Expression and Crystallization. cDNA encoding wild-type APS kinase from *P. chrysogenum* was cloned into an *E. coli* pET vector expression system (Novagen, Madison, WI) and expressed and purified as described previously (*8*). After purification, the enzyme was dialyzed extensively against 10 mM Na HEPPS buffer (pH 8.0) and then concentrated by membrane filtration to 10 mg of protein/mL. The protein (at a final concentration of >5 mg/mL) was crystallized by hanging-drop vapor diffusion and by micro batch methods at room temperature in 0.8−1.2 M Na^+/K^+ tartrate and 0.1 M Na MES (pH 6.0). Crystals of the trigonal space group $P3_121$ typically appeared overnight and often grew to 1.0 mm × 1.0 mm × 1.0 mm. These crystals had a V_M coefficient of 3.0 $Å^3$/Da (59% solvent) assuming one monomer per asymmetric unit and the following unit cell parameters: $a = b = 85.95$ Å and $c = 72.34$ Å. Despite the large size of the trigonal crystals, they did not diffract X-rays beyond 2.7 Å resolution.

Addition of polyethylinimine (0.5% final concentration) to the above conditions induced APS kinase to crystallize in orthorhombic space group $C222_1$ with a V_M of 2.5 $Å^3$/Da (51% solvent assuming one homodimer per asymmetric unit) and the following unit cell parameters: $a = 78.86$ Å, $b = 83.48$ Å, and $c = 141.95$ Å. The orthorhombic crystals grew much more slowly than the trigonal forms, typically appearing only after several weeks, and often as clusters of stacked plates. However, a few large single crystals were eventually obtained and were found to diffract X-rays to significantly higher resolution than the trigonal form. The orthorhombic crystals were ultimately used to determine the final structure.

Data Collection and Phase Determination. The structure of APS kinase was first determined by MIR methods using crystals of space group $P3_121$. This crystal form was chosen for our heavy atom derivative search because of the ease with which crystals could be obtained. All heavy atom soaks were conducted at room temperature in 1.2 M Na^+/K^+ tartrate and 0.1 M Na MES (pH 6.0). Native and derivative data were collected on a Siemens Hi-Star area detector mounted on a Rigaku rotating anode generator. Data were processed with XDS (*9*) and scaled with ROTAVATA/AGROVATA (*10*). Heavy atom positions were determined by inspection of difference Patterson maps and difference Fourier maps. The positions were refined and MIR phases calculated using the program PHASES (*11*). A 2.0 Å resolution native data set, from the orthorhombic crystal, was collected on Beamline 9-1 at SSRL and processed with DENZO and SCALEPACK (*12*). Table 1 lists data collection and processing statistics.

Table 1: Data Collection, Phasing, and Refinement Statistics

	native	native	phenyl-Hg	$ReCl_5$
space group	$C222_1$	$P3_121$	$P3_121$	$P3_121$
X-ray source	SSRL	CuKα	CuKα	CuKα
wavelength (Å)	0.98	1.54	1.54	1.54
resolution (Å)	2.0	3.0	2.8	3.0
no. of reflections	109188	19508	16706	15909
no. of unique reflections	31625	6148	7469	6458
completeness (%)	98.7	96.5	94.4	99.0
R_{merge}[a] (%)	4.3	7.9	4.3	6.1
heavy atom concentration (mM)			0.5	2.0
soaking time (Days)			12	2
no. of sites (ASU)			1	1
R_{iso}[b] (%)			11.9	11.9
phasing power[c]			2.71	1.47
figure of merit			0.705	
Refinement Statistics				
resolution (Å)	30.0−2.0			
no. of reflections ($\|F\| \geq 0$)	31625			
R-factor[d]	20.7			
R_{free}[d] (5% data)	24.9			
rms for bond distances (Å)	0.018			
rms for bond angles (deg)	1.80			
no. of non-hydrogen protein atoms	2800			
no. of water molecules	198			
no. of tartrate atoms (one molecule)	10			

[a] $R_{merge} = [\Sigma_h\Sigma_i|I_h - I_{hi}|/\Sigma_h\Sigma_i I_{hi}] \times 100$, where I_h is the mean of the I_{hi} observations of reflection h. [b] $R_{iso} = \Sigma|F_{PH}| - |F_P|/\Sigma|F_{PH}| \times 100$. [c] Phasing power $= \{\Sigma_h|F_{H(calc)}|^2/\Sigma_h[|F_{PH(obs)}| - |F_{PH(calc)}|]^2\}^{1/2}$. [d] R-Factor and R-free $= \Sigma||F_{obs}| - |F_{calc}||/\Sigma|F_{obs}| \times 100$ for 95% of the recorded data (R-factor) or 5% of the data (R-free).

Model Building and Refinement. The initial solvent-flattened MIR map was used to build a partial model of a single APS kinase subunit. Model building was carried out using the molecular graphics program O (*13*). After several rounds of model building and refinement using TNT (*14*), the conventional R-factor dropped to 35% for all data recorded out to 2.9 Å resolution. This structure was then used as a search model in a 2.0 Å resolution synchrotron data set from an orthorhombic $C222_1$ crystal (see above) using the molecular replacement program AMoRe (*10, 15*). Two equivalent peaks were found in the rotation and translation searches that corresponded to the two copies (one homodimer) in the asymmetric unit. After a single round of rigid-body refinement, the molecular replacement solution had an R-factor of 40.6% and a correlation coefficient of 65.8 for data between 10 and 4.0 Å resolution.

The molecular replacement solution of the orthorhombic data set was used to complete all ordered regions of the APS kinase dimer. Initially, after each round of model building, the structure was refined using 95% of the data to 2.5 Å resolution with TNT (*14*) constraining strict noncrystallographic symmetry. Refinement lowered both the R-free (*16*) and R-factor at every stage and improved most of the poorly defined electron density. However, at no time was any clear density observed for residues 149−169 in either subunit in the asymmetric unit. The structure was then refined with the simulated annealing algorithm in the program CNS (*17*) with high restraints placed on the noncrystallographic symmetry between the two subunits in the asymmetric unit. The resolution of the data was slowly extended with each round of refinement to a final resolution of 2.0 Å. The working and test data sets maintained the same lower-resolution

reflections upon extension. At every stage of refinement, the weight placed on the noncrystallographic symmetry restraint was reevaluated to give the lowest *R*-free value. It was observed that as the model improved, the noncrystallographic weight that gave the lowest *R*-free decreased. Once the *R*-free was less than 27%, noncrystallographic symmetry restraints were released, resulting in lower *R*-free values. Refinement was completed, resulting in a final *R*-factor of 20.7% and a final *R*-free of 24.9% for all recorded data to 2.0 Å resolution. A total of 89.1% of the residues fall within the most favored region of a Ramachandran plot, and none of the residues were in the disallowed region as determined by the program PROCHECK (*18*, *19*). Final refinement statistics are listed in Table 1.

Limited Proteolysis with Trypsin. Approximately 1 mg of pure APS kinase was incubated with about 0.2 μg of trypsin in 1 mL of 50 mM Tris-HCl buffer (pH 8.0) in the absence and presence of known ligands. The reaction was quenched by addition of gel loading buffer containing SDS and DTT and the mixture boiled in a water bath. The samples were then subjected to discontinuous electrophoresis on a 20% homogeneous polyacrylamide gel (*20*).

RESULTS

Crystallographic Properties. In the absence of ligands, APS kinase crystallized into two different space groups: $P3_1$-21 and $C222_1$. The structure of the enzyme was initially determined by MIR methods to 2.9 Å resolution in the trigonal crystal form. This solution had one APS kinase monomer in the asymmetric unit. The monomer of one asymmetric unit made significant crystal contacts with the monomer in an adjacent asymmetric unit, forming an APS kinase homodimer with the dimer 2-fold symmetry axis coincident with the crystallographic 2-fold axis. The structure of APS kinase was also determined by molecular replacement (using the first model described above) in the orthorhombic crystal form. This solution had one APS kinase homodimer per asymmetric unit with the two polypeptide chains designated as A and B. The homodimers observed in the orthorhombic crystals and the trigonal crystals superimpose almost perfectly onto one another with only slight deviations due to crystal contacts. The structure of APS kinase reported here was refined against a 2.0 Å resolution data set from a single orthorhombic crystal collected at a synchrotron radiation source. The final conventional *R*-factor and *R*-free of the reported refined model are 20.7 and 24.9%, respectively. The crystallographic data and refinement statistics are summarized in Table 1. The final model consists of residues 8−143 and 170−210 of the A subunit and residues 8−148 and 170−210 of the B subunit. The remaining residues did not have clearly defined electron density with which to ascertain their position.

The average temperature factor of the A subunit is 40.4 Å^2. The B subunit had consistently higher temperature factors with an average of 50.4 Å^2. The difference in temperature factors between the two copies in the asymmetric unit can be attributed to the crystal contacts that each subunit makes. A subunits pack mostly only against the A subunits of adjacent asymmetric units, while B subunits contact mostly only other B subunits. The A subunits appear to pack tighter, making more crystal contacts than B subunits in the crystal lattice, resulting in an overall lower temperature value.

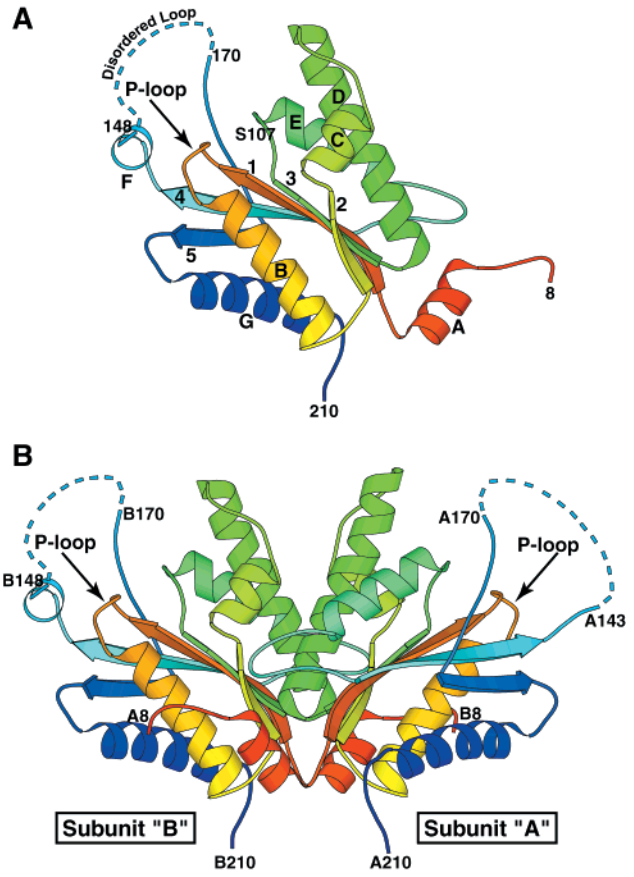

FIGURE 1: Structure of *P. chrysogenum* APS kinase. (A) The polypeptide chain of a single APS kinase subunit (as it exists in the dimer) is traced in a rainbow-colored ribbon format starting with red at the N-terminus and ending with blue at the C-terminus. The enzyme subunit is composed of a five-stranded parallel β-sheet and seven α-helices. The five strands are numbered sequentially as they occur in the primary sequence. The α-helices, which pack against the sheet, are labeled alphabetically starting with A at the N-terminus. Residues 148 and 170 delineate the ends a 21-residue stretch of the enzyme that is disordered in both subunits (dashed line). (B) APS kinase dimer. The ribbon is color-coded as described for panel A. The final model consists of residues 8−143 and 170−210 of the A subunit and residues 8−148 and 170−210 of the B subunit. Residues 143−149 in the B subunit (preceding the disordered loop) form one turn of an α-helix (αF), which is disordered in the A subunit. The dimer structure results in two active sites identified by their P-loops. This figure was generated using the program MOLSCRIPT (*39*).

Overall Structure. As shown in Figure 1, the APS kinase subunit folds into a classic α/β purine nucleotide binding motif (*21*). This structure consists of an open five-stranded parallel β-sheet that is sandwiched between two α-helical bundles. In APS kinase, the β-sheet is composed mainly of hydrophobic residues that pack against predominantly hydrophobic residues of amphiphilic α-helices to form the core of each subunit. A sequence alignment of APS kinases from a variety of organisms with the secondary structure elements observed in the fungal enzyme (Figure 2) suggests that the basic structure of the enzyme is highly conserved. For the most part, deviations among species are seen only in the N- and C-termini and in the extended loops, such as the αE−β4 loop in the fungal enzyme (residues 122−132), which has no counterpart in the enzyme from nonfungal sources.

Active Site Region. The absence of bound substrates in the X-ray-derived structure prevents us from identifying the

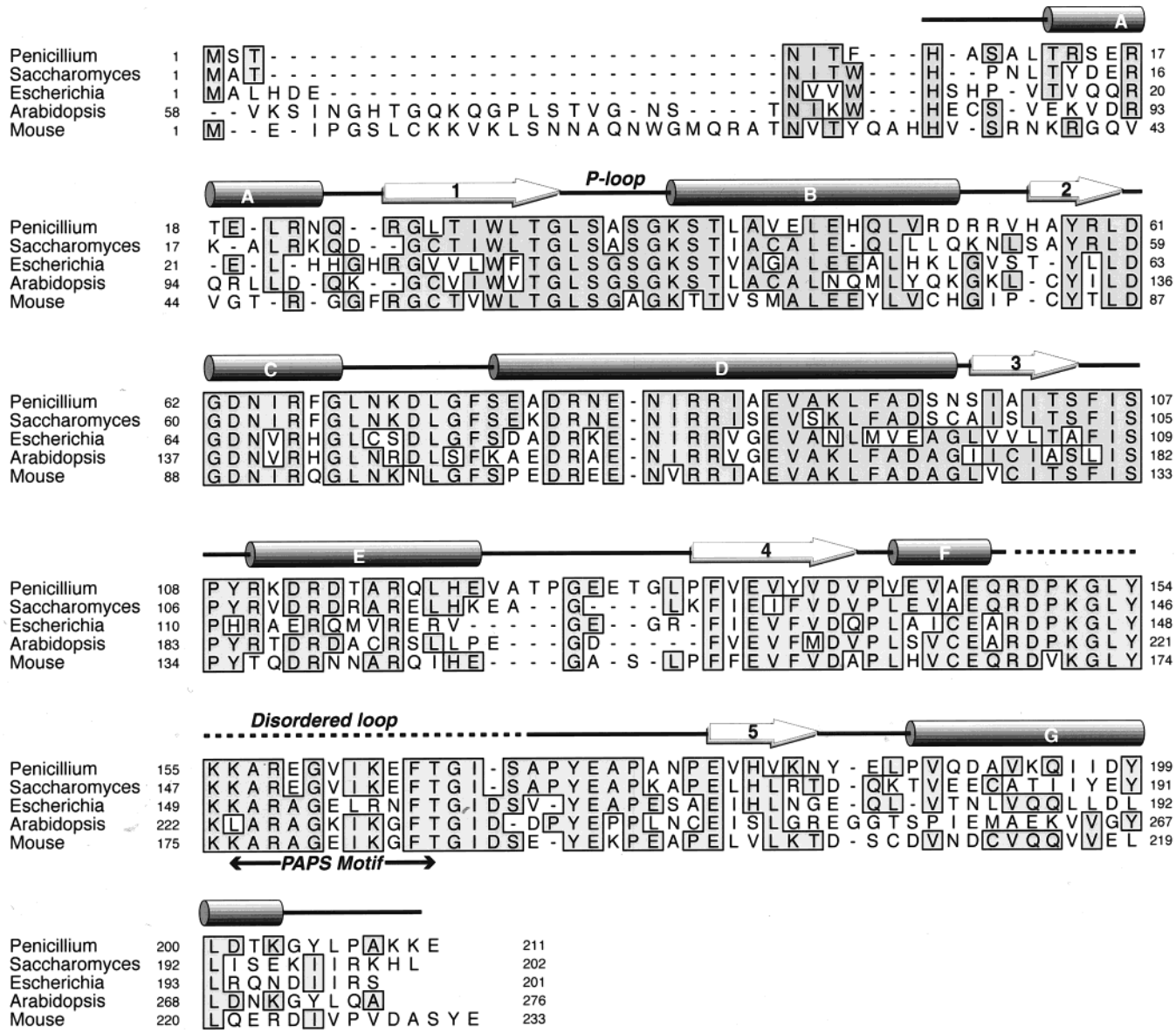

FIGURE 2: Primary sequences of APS kinases from several organisms and the corresponding secondary structure of the *P. chrysogenum* enzyme. The structural elements are indicated as follows: cylinder = α-helix, arrow = β-strand, line = loop or coil, and dashed line = disordered region. The active site P-loop and the region implicated in binding (P)APS are denoted.

residues involved in catalysis by APS kinase. However, the structure of the free enzyme in combination with known sequence motifs and crystal structures of other mononucleotide kinases allows us to infer that the catalytic site lies in the vicinity of the Walker A (kinase 1a) motif, ^{32}GLSASGKS^{39}, which forms a characteristic P-loop structure (*22*−*24*). This structure, located between β1 and αB (Figure 1), has been observed in a variety of mononucleotide binding proteins, G proteins, and motor proteins, and is used to form a large "anion hole" that accommodates the phosphate groups of the nucleoside triphosphate (*24*−*26*).

Satischandran et al. (*7*) reported that Ser 109 of the *E. coli* APS kinase served as an intermediary acceptor in the overall transfer of a phosphoryl group from MgATP to APS. However, mutation of the homologous Ser 107 of the fungal enzyme to Ala or Cys did not eliminate activity, although chemical modification of the sole Cys residue in the Ser 107 Cys mutant inactivated the enzyme (*8*). MgATP, MgADP, or APS (in the presence of MgADP) protected the enzyme from modification and inactivation. These results suggested that the mechanism of the fungal enzyme does not include a Ser 107 P intermediate, but that Ser 107 probably resides close to the substrate binding pocket. The crystal structure confirms this prediction. As seen in Figures 1 and 3, Ser 107 is located on the conserved loop between β3 and αE with its hydroxyl group 9 Å away from the ϵ-amino of P-loop Lys 38.

Prior to obtaining any structural information, we wondered whether the sequence ^{135}EVYVD^{139} played a role in substrate binding. This stretch, which is conserved among APS kinases, is similar to the Walker B (kinase 2) motif (*22*, *23*). In all previous structures of proteins involving P-loop-mediated binding to MgATP, the Walker B motif resides in the β-strand adjacent to the P-loop. The conserved Asp hydrogen bonds to one of the water molecules surrounding the Mg^{2+} of MgATP (*24*). In APS kinase, however, ^{135}EVYVD^{139} is located on strand β4, which is positioned on the opposite side of the P-loop. Consequently, Asp 139 cannot interact directly with bound MgATP. Thus, ^{135}EVYVD^{139} is unlikely to be a Walker B motif. For similar

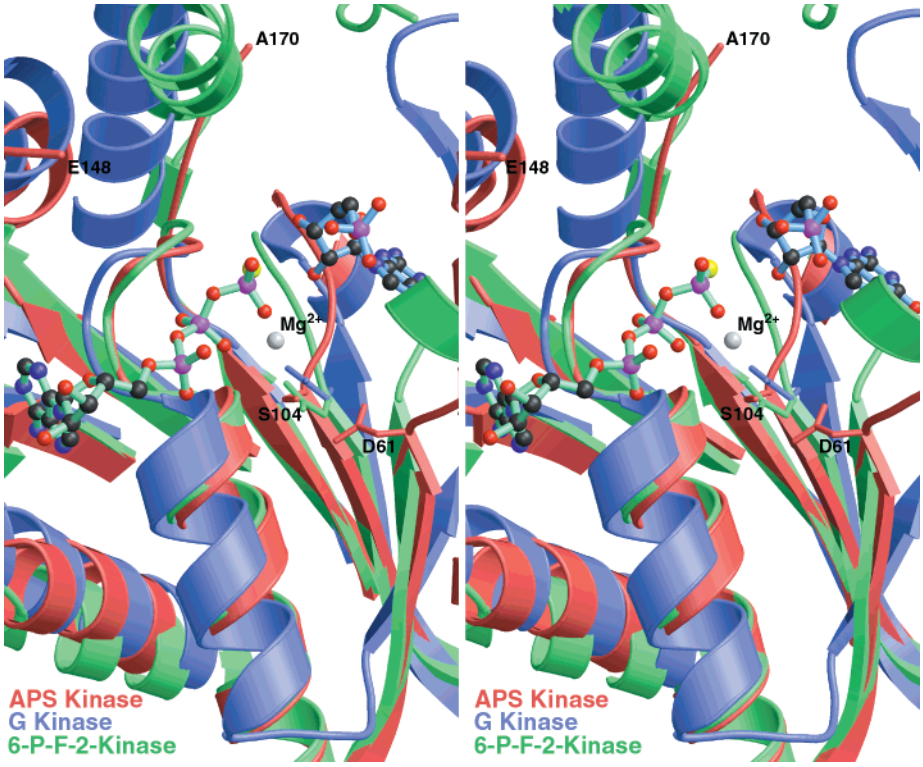

FIGURE 3: Stereo superposition of the P-loop active site region. Shown are the active site regions from the enzymes APS kinase (red) and guanylate kinase (blue) and the 6-phosphofructo-2-kinase domain (green) of the bifunctional enzyme 6-phosphofructo-2-kinase/fructose-2,6-bisphosphatase. Also shown is the ATP-γ-S (ball-and-stick model with green bonds) as observed in the 6-phosphofructo-2-kinase domain and the GMP (ball-and-stick model with blue bonds) seen in guanylate kinase. The binding of these two substrates in their respective enzymes provides clues to the location of the substrate binding sites in APS kinase. This figure was generated using the program MOLSCRIPT (*39*) and rendered by Raster3D (*40*).

reasons, the sequence ^{149}DXXG^{152} probably plays no role in nucleotide binding by APS kinase (Figure 1).

Superposition of the APS kinase active site region onto other P-loop-containing mononucleotide kinases, G proteins, and motor proteins revealed that Ser 104 structurally substitutes for the normally conserved aspartate of the Walker B motif found in these other proteins (Figure 3). However, these residues are not functionally equivalent. When Ser 104 was replaced with Ala, the mutant enzyme was fully active and actually had a higher affinity for APS than the wild-type enzyme (*8*). Thus, Ser 104 is not essential for substrate binding or catalysis. The X-ray structure of bovine mitochondrial F1-ATPase (*27*) may be more relevant because its Walker B Asp maps to Asp 61 of APS kinase, a residue universally conserved in all APS kinases. Asp 61 resides next to Ser 104, but in the adjacent strand (Figure 3) and, consequently, is too far removed (at least, in the free enzyme) to hydrogen bond to a water molecule surrounding the Mg^{2+}. But the APS kinase structure can accommodate slight movement around Asp 61 (the β2−αC loop should be somewhat flexible). Such a conformational change induced by MgATP binding could position APS-binding residues in a pocket formed by helices αC−αE (Figure 3). The Mg^{2+}-induced conformational change required for APS binding is corroborated by the observation that the APS binding affinity decreases >100-fold when APS kinase is bound to ADP in the absence of Mg^{2+} (*3*). The location of the putative APS binding subsite is similar to those of the acceptor substrates in adenylate kinase and guanylate kinase (*28*, *29*), i.e., in other enzymes that catalyze the phosphorylation of mononucleotides (Figure 3). An induced conformational change triggered by Asp 61 interacting with MgATP may also serve as the basis of the obligatory ordered binding of substrates (MgATP before APS). Attempts to diffuse MgADP alone or with APS resulted in crystal disintegration of both APS kinase crystal forms, suggesting large conformational changes upon binding substrates, subsequently disrupting vital crystal contacts.

Disordered Region. The most striking feature of the ligand-free structure is that residues 149−169 are completely disordered in both subunits. At no time during refinement was there any clear and contiguous electron density for any of the 21 residues in either subunit. The lack of order in this region was also observed in the structure determined in the trigonal space group with only one subunit per crystallographic asymmetric unit. In the B subunit, residues 142−147 form one turn of an α-helix (αF) before the electron density diminishes (in the A subunit, the last ordered residue is 143). This suggests that the first part of the disordered region may form a longer helix as is observed in the structurally homologous adenylate kinase, guanylate kinase, and thymidine kinase. In these enzymes, the region that is topologically equivalent to the APS kinase disordered region extends over the P-loop and makes contact with both the nucleoside triphosphate donor and the phosphoryl acceptor (*29*−*31*). Thus, it may be no coincidence that the disordered region of APS kinase contains ^{156}KAREGVIKEFT^{166}, a sequence present in several (P)APS-binding enzymes (*7*). We suggest that the high degree of flexibility in this region is not a crystallization artifact but, rather, is a reflection of

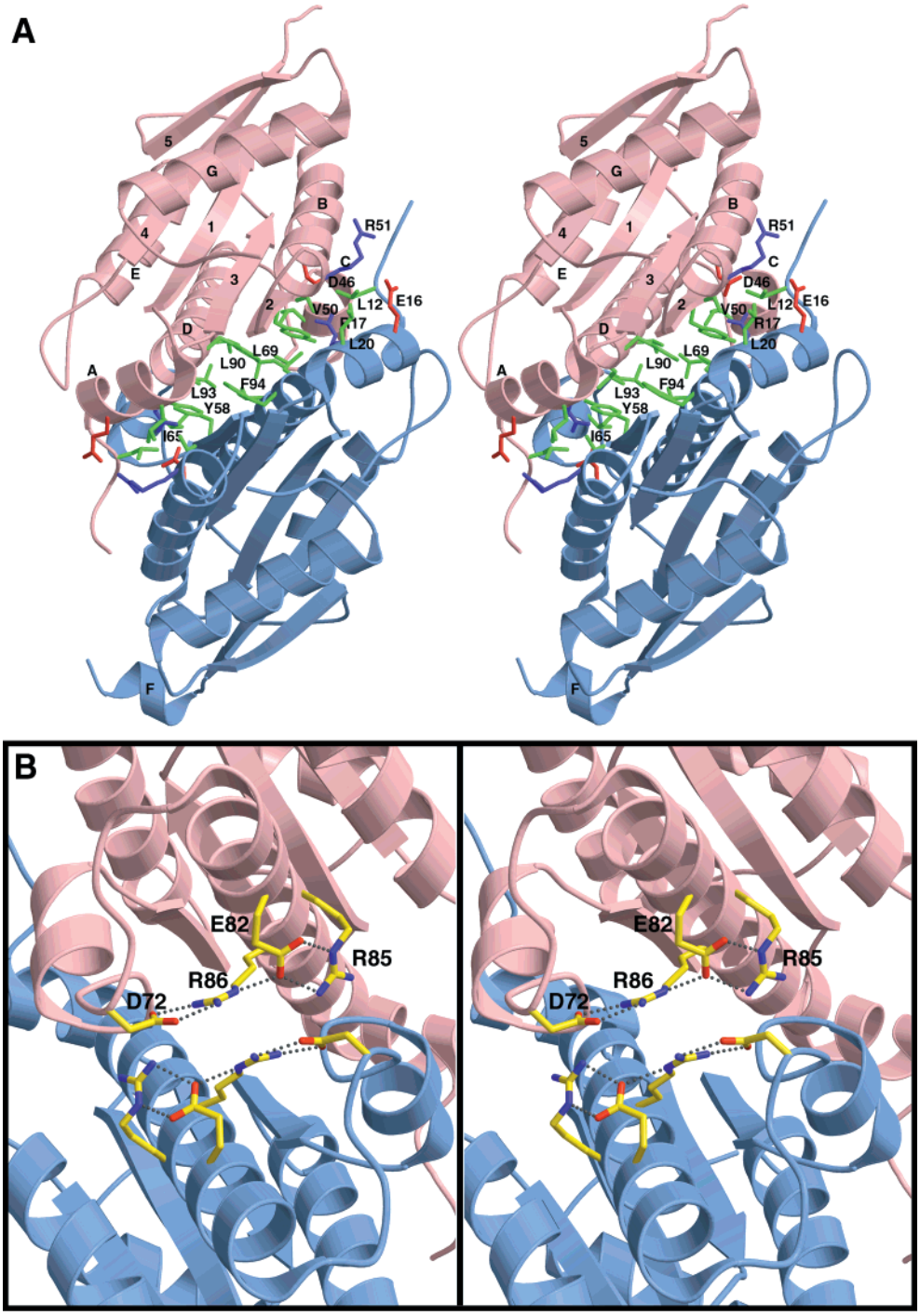

FIGURE 4: Dimer interface. (A) Stereoview of the APS kinase dimer highlighting residues that stabilize the interface. The view is looking up the dimer 2-fold axis from the "bottom". The A and B subunits are colored red and blue, respectively. The residues interacting across the dimer interface are color-coded as follows: green = hydrophobic, red = acidic, and blue = basic. (B) Closeup "top" view of charged residues lying near the dimer interface that form intrasubunit salt bridges. The view is approximately down the 2-fold axis but rotated 180° around the vertical axis from the view in panel A. These subunits have the potential to form an intersubunit salt bridging network by rotation of side chains. The A and B subunits are colored red and blue, respectively, and the charged residues in the A subunit are labeled. This figure was generated with the program MOLSCRIPT (*39*) and rendered by Raster3D (*40*).

the ordered binding mechanism. That is, this region, which may harbor part of the APS subsite, *is* highly disordered in the free enzyme.

APS Kinase Dimer. The crystallographic homodimer is consistent with studies on native APS kinase in solution (*1*). Although several other members of the α/β purine nucleotide binding superfamily form dimers (e.g., 6-phosphofructo-2-kinase and thymidine kinase), the APS kinase dimer interface appears to be unique. As shown in Figures 1B and 4, the major intersubunit contacts are made between portions of α-helices C and D packing together with β-strands 2 and 3. Also, helices αA and αB of opposite subunits pack together.

The dimeric structure is stabilized by hydrophobic interactions and salt linkages (Figure 4). Residues Ile 65, Leu 69, Val 90, and Leu 93 in helices αC and αD of both subunits pack together at the dimer interface, forming a hydrophobic pocket. Phe 94 and Tyr 58 reside at the bottom of this pocket adjacent to the dimer 2-fold axis, resulting in a cluster of

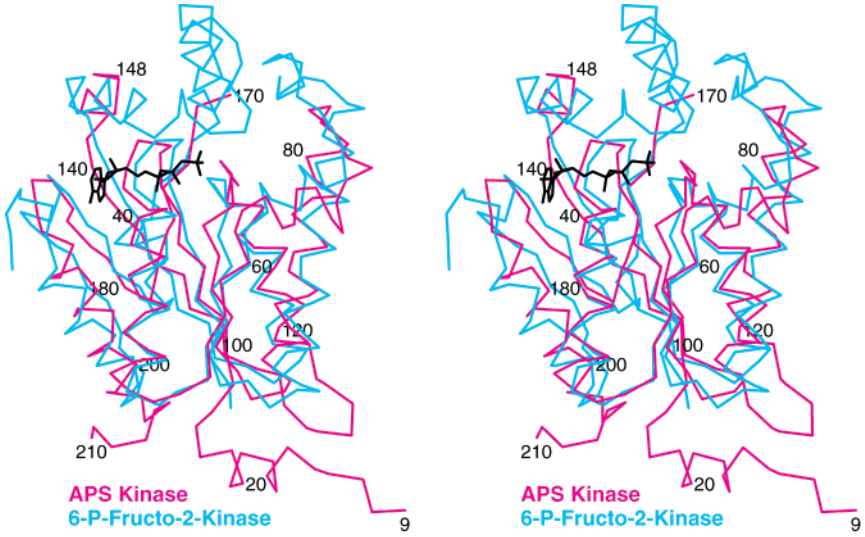

FIGURE 5: Stereoview showing the superposition of the polypeptide backbone structures of APS kinase (magenta) and the homologous 6-phosphofructo-2-kinase domain (cyan). The latter is shown with bound ATP (shown in black). The rms deviation for 131 equivalent C-α positions is 2.6 Å. This figure was generated using the program MOLSCRIPT (*39*).

four aromatic side chains. These four hydrophobic residues form a π stacking ladder across the interface with a distance of ~3.7 Å between the parallel aromatic side chains (Figure 4A). Other small hydrophobic pockets are made between Val 50 and Leu 12 of one subunit and Leu 20 of the other. Most of these hydrophobic residues are conserved in all APS kinases and would be solvent-exposed if the dimer were dissociated. The total buried accessible surface area at the dimer interface is 1700 Å^2, suggesting that there is also a good deal of van der Waals packing between the two subunits.

Although the N-terminal end of helix αD contains several charged residues that are positioned close enough to the subunit interface to make dimer-stabilizing contacts, in the free enzyme, they form intrasubunit salt bridges. Arg 85 and Asp 82 of the same subunit form a salt link, as do Arg 86 and Asp 72 (Figure 4B). All four residues lie at the N-terminal of αD near the dimer 2-fold axis, resulting in a cluster of eight charge residues that could easily salt link to residues across the dimer. These intrasubunit interactions could possibly help stabilize the monomer structure prior to dimer formation. There are only four intersubunit salt bridges in the free enzyme. These are between Glu 16 and Arg 51, and between Arg 17 and Glu 46 (Figure 4A).

It is still uncertain how the association of monomers contributes to the formation of a competent active site region. The structures shown in Figures 1 and 4 together with homology considerations (see below) eliminated one possibility, viz., that the active site resides at the subunit interface.

Structural Homologues. The C-α backbone of APS kinase was used as a search model to probe a three-dimensional structural database to find its closest relative (*32*). As a member of the purine nucleotide-binding superfamily of protein folds, it was expected that APS kinase would have a large number of structural homologues. The kinase domain of the bifunctional enzyme 6-phosphofructo-2-kinase/2,6-phosphofructo-2-phosphatase had the closest similarity with an rms deviation of 2.6 Å for 131 equivalent C-α positions (Figure 5). The sequences of these two proteins are only 9% identical, but the similarity in structure is not surprising. Both enzymes catalyze the transfer of the γ-phosphoryl group from ATP to a hydroxyl group of a furanose ring sugar. By examination of these two structures, it is clear that the greatest change that occurs upon ATP binding is localized to the region corresponding to disordered residues 149−169 in APS kinase. (The disordered region of APS kinase and the corresponding region in 6-phosphofructo-2-kinase have different compositions, but are similar in length.) It has been suggested that this motion shields the bound MgATP from bulk water, thereby reducing futile ATP hydrolysis (*26*). The high mobility of this region is consistent with the high degree of disorder that we detected in the X-ray structure of unliganded APS kinase. The E·MgATP complex of 6-phosphofructo-2-kinase very likely provides a glimpse of what APS kinase may look like when complexed with MgATP (Figures 3 and 5).

A variety of other kinases that catalyze the phosphorylation of small molecules are also closely related structurally to APS kinase. These include deoxynucleoside monophosphate kinase (with an rms deviation of 2.9 Å for 129 C-α atoms), adenylate kinase (3.0 Å for 135 C-α atoms), guanylate kinase (3.1 Å for 126 C-α atoms), and thymadine kinase (3.5 Å for 129 C-α atoms).

Limited Proteolysis and Protection by Ligands. If, as the X-ray structure suggests, the disordered region of APS kinase is flexible and solvent-exposed, then this part of the enzyme should be highly accessible to a protease in solution. Furthermore, if the binding of MgATP or MgADP causes this region to assume a more highly structured state, then either of these nucleotides should protect this region from proteolysis.[2] Figure 6 shows the results of an experiment in which APS kinase was incubated with a small quantity of trypsin in the presence and absence of various ligands. In the absence of ligands, the enzyme is cleaved rapidly, producing a fragment that is about 5−6 kDa smaller than

[2] It should be noted that the proteolysis experiments were also motivated by an earlier observation that the APS kinase-like, C-terminus of fungal ATP sulfurylase is rapidly cleaved by low levels of trypsin at a position corresponding to Lys 163 in true APS kinase. This initial cleavage was followed by another at the position corresponding to Arg 117 (L. Daly, I. J. MacRae, and I. H. Segel, unpublished results).

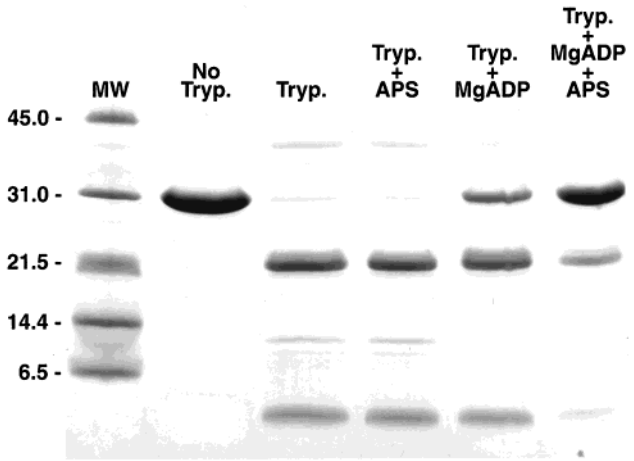

FIGURE 6: Protection against limited proteolysis of APS kinase by trypsin (Tryp.). The digestion patterns after incubation for 90 min in the presence of the indicated additions are shown. Preliminary experiments established that a 90 min digest resulted in most of the original enzyme being cleaved (data not shown). The incubation mixture contained APS kinase (1 mg/mL) and trypsin (0.2 μg/mL) in 0.05 M Tris-HCl buffer (pH 8.0). Each lane was loaded with the equivalent of 2 μg of APS kinase. MgADP and APS concentrations were 10 and 0.1 mM, respectively, when indicated. Protection by MgATP alone was identical to that provided by MgADP without APS (not shown). Molecular mass standards are shown (lane 1) with their respective mass in kilodaltons. APS kinase, whose calculated molecular mass is 23.7 kDa, runs anomalously high (lane 2). N-Terminal sequence analysis of the ~22 and ~5 kDa fragments verifies trypsin cleavage occurs at Arg 158.

the whole enzyme (Figure 6, lane 3). The size reduction is consistent with cleavage at a site somewhere between Arg 148 and Lys 163, i.e., within the disordered region. N-Terminal sequence analyses of the major band (~22 kDa) yielded STNITFHA, i.e., the N-terminal sequence of the original enzyme minus Met 1 (Figure 2). N-Terminal sequencing of the ~5 kDa cleavage product yielded EGXIKEFT. These results confirm that the primary cleavage occurred at Arg 158 in the disordered loop and not 5−6 kDa in from the N-terminus. As shown in Figure 6, MgADP provided partial protection against cleavage (MgATP behaved just like MgADP; data not shown). APS alone had no effect, but augmented the protection provided by MgADP. The results are consistent with both the steady state kinetics of the APS kinase reaction (*2*) and various binding studies (*3*, *4*) which show that APS binds only to the E·MgATP or E·MgADP complex.

DISCUSSION

The kinetic mechanism of *P. chrysogenum* APS kinase has been shown to be obligatory ordered; MgATP (or MgADP) adds before APS, and PAPS dissociates before MgADP (*2*, *33*). Inactivation protection studies (*3*) and direct equilibrium binding studies (*4*) indicated that the ordered sequence was structurally based, not simply a kinetic phenomenon. For example, in the absence of MgATP or MgADP, no APS binding could be detected even at APS concentrations up to 1 mM. However, in the presence of 5 mM MgADP, APS binds with an apparent K_d of ca. 2 μM. The structure of APS kinase presented in this report supports the suggestion that structural changes underlie the ordered binding. The relevant observations are that (a) the MgATP-binding P-loop structure is well-defined. However, (b) residues 149−169 are disordered in both copies of the asymmetric unit. This disordered region contains the putative APS binding sequence (^{156}KAREGVIKEFT^{166}) (*7*).

A high degree of flexibility of the disordered region is supported by protease-sensitivity studies. In the absence of any ligands, the enzyme is readily cleaved by trypsin at Arg 158. But in the presence of MgATP or MgADP, the region was protected. APS alone had no effect, but enhanced the protection provided by MgADP.

We suggest the following plausible model. The disorder of the stretch of residues 149−169 reflects a high degree of flexibility of this region and is responsible for the absence of a functional APS binding site on the free enzyme. MgATP binding to the P-loop concomitantly triggers (a) a displacement of Asp 61 (to stabilize the E·MgATP complex) and (b) a movement of the disordered region that results in the formation of a functional APS subsite in a pocket located between helices αC−αE (Figure 3). When both substrates are bound, the (now, highly ordered) stretch of residues 149−169 behaves as a lid to cover the active site. The lid itself may contain residues that bind APS, thereby contributing to the stability of the ternary E·MgATP·APS complex. This scenario is reminiscent of the domain-closure mechanism observed in substrate binding to adenylate kinase (*30*). The structural changes proposed for the fungal enzyme, however, may not be able to be applied to APS kinases from all sources. For example, the *E. coli* enzyme is reported to bind APS in the absence of MgATP (*5*, *6*).

In animals, ATP sulfurylase and APS kinase reside on a single (bifunctional) polypeptide chain with a structure that has been described schematically as ^{1}APS−kinase^{199}−^{200}linker^{236}−^{237}ATP−sulfurylase^{624} (*34*). Deyrup et al. reported that the expressed bifunctional mouse protein displayed no significant APS kinase activity (a) if the kinase domain (APSK) was expressed independently of the downstream "linker" and sulfurylase (ATPS) domains, (b) if the kinase and sulfurylase domains were joined without the "linker" region, or (c) if the two domains were rearranged without the "linker" (i.e., ATPS−APSK). The latter construct resembles the fungal ATP sulfurylase (*35*), except that in the fungal protein, the APS kinase-like domain has no kinase activity; it serves solely as an allosteric domain for binding PAPS (*36*). If the structure of mouse APS kinase in the region of residues 200−230 is similar to that of the fungal enzyme (in the corresponding stretch of residues 180−211), then the absence of APS kinase activity in the constructs of the mouse enzyme lacking residues 200 to ca. 230 is not unexpected. That region may not be a linker but, rather, an integral part of the enzyme that is homologous to strand β5, and helix αG of the fungal enzyme. Examination of 16 published sequences of APS kinases shows only a low level of identity in this region, but a degree of similarity suggesting that this region is an important part of the enzyme from all sources.

APS kinase from *P. chrysogenum* contains no sulfur amino acids except for the N-terminal Met. Plant APS kinases, on the other hand, contain from four to eight Cys residues per subunit. A sulfhydryl−disulfide interconversion (*37*) mediated by thioredoxin (*38*) may regulate APS kinase in plants. If this is the case, the structure of *P. chrysogenum* APS kinase suggests that the Cys residues involved in this redox process are Cys 132 and Cys 176. These are the only two Cys residues close enough together in *Arabidopsis* APS kinase

to form an intrasubunit disulfide bond. (The α-carbons are 5.8 Å apart. All others are >10 Å apart.)

ACKNOWLEDGMENT

We thank the Protein Structure Lab at the University of California, Davis, for sequence analysis. Some of the work reported here was performed at SRRL, which is operated by the Department of Energy, Office of Basic Energy Sciences. The SSRL Biotechnology Program is supported by the National Institutes of Health, National Center for Research Resources, Biomedical Technology Program, and by the Department of Energy, Office of Biological and Environmental Research.

REFERENCES

1. Renosto, F., Seubert, P. A., Knudson, P., and Segel, I. H. (1985) *J. Biol. Chem. 260*, 1535−1544.
2. Renosto, F., Seubert, P. A., and Segel, I. H. (1984) *J. Biol. Chem. 259*, 2113−2123.
3. Renosto, F., Seubert, P. A., Knudson, P., and Segel, I. H. (1985) *J. Biol. Chem. 260*, 11903−11913.
4. Renosto, F., Martin, R. L., and Segel, I. H. (1991) *Arch. Biochem. Biophys. 284*, 30−34.
5. Satishchandran, C., and Markham, G. D. (1989) *J. Biol. Chem. 264*, 15012−15021.
6. Satishchandran, C., and Markham, G. D. (1990) *FASEB J. 4*, A2119 (abstract 2467).
7. Satishchandran, C., Hickman, Y. N., and Markham, G. D. (1992) *Biochemistry 31*, 11684−11688.
8. MacRae, I., Rose, A. B., and Segel, I. H. (1998) *J. Biol. Chem. 273*, 28583−28589.
9. Kabsch, W. (1988) *J. Appl. Crystallogr. 21*, 916−924.
10. Collaborative Computational Project 4 (1994) *Acta Crystallogr. D50*, 760−763.
11. Furey, W., and Swaminathan, S. (1997) *Methods Enzymol. 277*, 590−620.
12. Otwinowski, Z., and Minor, W. (1997) in *Methods in Enzymology* (Carter, C. W., Jr., and Sweet, R. M., Eds.) pp 307−326, Academic Press, New York.
13. Jones, T. A., Zou, J. Y., Cowan, S. W., and Kjeldgaard, M. (1991) *Acta Crystallogr. A47*, 110−119.
14. Tronrud, D. E., Ten-Eyck, L. F., and Matthews, B. W. (1987) *Acta Crystallogr. A43*, 489−501.
15. Navaza, J. (1993) *Acta Crystallogr. D49*, 588−591.
16. Brünger, A. T. (1993) *Acta Crystallogr. D49*, 24−36.
17. Brünger, A. T., Adams, P. D., Clore, G. M., DeLano, W. L., Gros, P., Grosse-Kunstleve, R. W., Jiang, J.-S., Kuszewski, J., Nilges, M., Pannu, N. S., Read, R. J., Rice, L. M., Simonson, T., and Warren, G. L. (1998) *Acta Crystallogr. D54*, 905−921.
18. Laskowski, R. A., MacArthur, M. W., Moss, D. S., and Thornton, J. M. (1993) *J. Appl. Crystallogr. 26*, 283−291.
19. Ramakrishnan, C., and Ramachandran, G. N. (1965) *Biophys. J. 5*, 909−933.
20. Laemmli, U. K. (1970) *Nature 227*, 680−685.
21. Schulz, G. E., and Schirmer, R. H. (1974) *Nature 250*, 142−144.
22. Walker, J. E., Saraste, M., Runswick, M. J., and Gay, N. J. (1982) *EMBO J. 1*, 945−951.
23. Traut, T. W. (1994) *Eur. J. Biochem. 222*, 9−19.
24. Smith, C. A., and Rayment, I. (1996) *Biophys. J. 70*, 1590−1602.
25. Dreusicke, D., and Schultz, G. E. (1986) *FEBS Lett. 208*, 301−304.
26. Schulz, G. E. (1992) *Curr. Opin. Struct. Biol. 2*, 61−67.
27. Abrahams, J. P., Leslie, A. G., Lutter, R., and Walker, J. E. (1994) *Nature 370*, 621−628.
28. Abele, U., and Schulz, G. E. (1995) *Protein Sci. 4*, 1262−1271.
29. Stehle, T., and Schulz, G. E. (1992) *J. Mol. Biol. 224*, 1127−1141.
30. Schlauderer, G. J., Proba, K., and Schulz, G. E. (1996) *J. Mol. Biol. 256*, 223−227.
31. Wild, K., Bohner, T., Folkers, G., and Schulz, G. E. (1997) *Protein Sci. 6*, 2097−2106.
32. Holm, L., and Sander, C. (1993) *J. Mol. Biol. 233*, 123−138.
33. MacRae, I. J., and Segel, I. H. (1999) *Arch. Biochem. Biophys. 361*, 277−282.
34. Deyrup, A. T., Krishnan, S., Singh, B., and Schwartz, N. B. (1999) *J. Biol. Chem. 274*, 10751−10757.
35. Foster, B. A., Thomas, S. M., Mahr, J. A., Renosto, F., Patel, H., and Segel, I. H. (1994) *J. Biol. Chem. 269*, 19777−19786.
36. Renosto, F., Martin, R. L., Wailes, L. M., Daley, L. A., and Segel, I. H. (1990) *J. Biol. Chem. 265*, 10300−10308.
37. Jender, H. G., and Schwenn, J. D. (1984) *Arch. Microbiol. 138*, 9−14.
38. Schwenn, J. D., and Schriek, U. (1984) *FEBS Lett. 170*, 76−80.
39. Kraulis, P. J. (1991) *J. Appl. Crystallogr. 24*, 946−950.
40. Merritt, E. A., and Murphy, M. E. P. (1994) *Acta Crystallogr. D50*, 869−873.

BI9924157